

pubs.acs.org/JACS Article

# Conjugation- and Aggregation-Directed Design of Covalent Organic Frameworks as White-Light-Emitting Diodes

Sizhuo Yang, Daniel Streater, Christian Fiankor, Jian Zhang, and Jier Huang\*



Cite This: J. Am. Chem. Soc. 2021, 143, 1061-1068



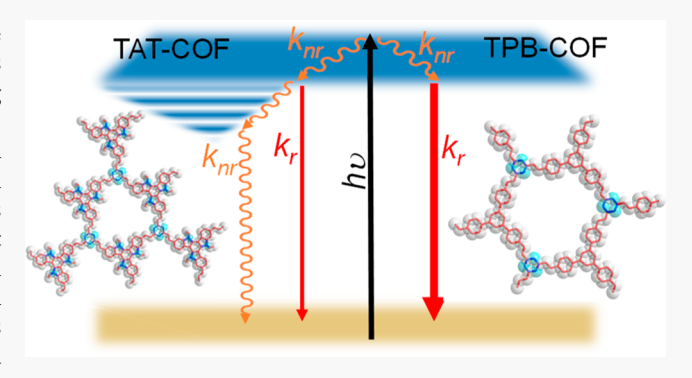
**ACCESS** 

Metrics & More



Supporting Information

ABSTRACT: 2D covalent organic frameworks (COFs) have emerged as a promising class of organic luminescent materials due to their structural diversity, which allows the systematic tuning of organic building blocks to optimize emitting properties. However, a significant knowledge gap exists between the design strategy and the fundamental understanding of the key structural parameters that determine their photophysical properties. In this work, we report two highly emissive sp²-C-COFs and the direct correlation of the structure (conjugation and aggregation) with their light absorption/emission, charge transfer (CT), and exciton dynamics, the key properties that determine their function as luminescent materials. We show that white light can be obtained by simply coating COFs on an LED strip or mixing the two COFs.



Using the combination of time-resolved absorption and emission spectroscopy as well as computational prediction, we show that the planarity, conjugation, orientation of the dipole moment, and interlayer aggregation not only determine the light-harvesting ability of COFs but also control the exciton relaxation pathway and photoluminescent quantum yield.

#### ■ INTRODUCTION

Organic luminescent materials have attracted increasing attention in the past decades because of their widespread applications in organic light-emitting diodes (OLEDs), 1-3 ultrasensitive sensors, 4,5 and bioimaging. 6,7 Since the first report of their use for efficient OLED devices, a variety of luminescent chromophores have evolved, which include smallmolecule and polymer emitters. 8-10 The small-molecule emitters typically have a precise molecular structure, an accessible structural modification, high purity, and luminescence efficiency. However, they often suffer from poor stability in the presence of air and humidity as well as a complicated fabrication process and heterogeneity when they are processed into films. 11-14 These issues can be solved by using polymer emitters, which are more favorable for wet processing and flexible production and may take advantage of the phenomenon called aggregation-induced emission (AIE) that results from a restriction of intramolecular rotations, vibrations, and motions. 15-17 However, the polymer emitters typically show lower emission efficiency in comparison to the small-molecule emitter, which may result from the imprecision of polymer chemistry (defects).

Given the capability to assemble molecular chromophores in a periodic crystalline framework and thereby integrate the beneficial features and overcome the drawbacks of molecular and polymer emitters, covalent organic frameworks (COFs) have emerged as a promising class of organic luminescent materials. <sup>18</sup> COFs are built from periodic multidentate organic

building blocks via covalent bonds. 19-23 The diverse options of organic ligands allow the inclusion of a large majority of available chromophore units without the worry of solubility and processability. 24-27 In addition, these ligands can be readily modified by introducing functional groups, which allows the systematic tuning of photophysical properties to optimize the emission efficiency. Meanwhile, the intrinsic ordered porosity of these materials may prevent aggregation of emitters and suppress nonradiative deactivation. As such, COFs can offer the same level of advantages as molecular emitters while retaining the stability of the solid-state emitters. Indeed, a few photoluminescent COFs have been reported recently. 24,28-40 For example, Jiang and co-workers pioneered the research to incorporate pyrene as building unit in COFs, <sup>28–33</sup> by which blue emission was achieved via exciton migration owing to the  $\pi$ - $\pi$  stacked columnar structure. In the meantime, emissive COFs have been designed by introducing intramolecular hydrogen bonding or AIEgens within the frameworks, 34-38 where the intramolecular rotation and vibration have been restricted, resulting in enhanced

Received: November 8, 2020 Published: January 4, 2021

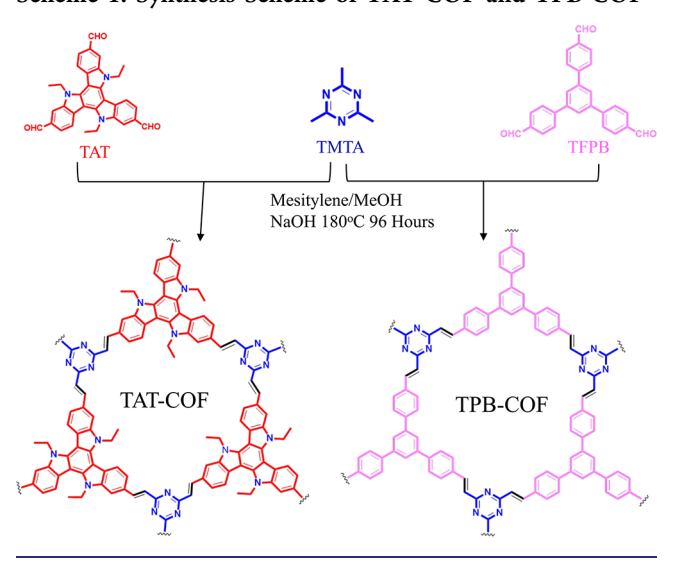




luminescence. More recently, an sp<sup>2</sup>-C-COF was reported to be highly emissive, <sup>39,40</sup> where the full  $\pi$  conjugation between the building blocks can facilitate exciton migration through the framework.

While these prior works demonstrate the great potential of COFs as organic luminescent materials, a significant gap exists between the rational design of COFs and the fundamental understanding on the key structural parameters that determine their light absorption and emission properties. In this work, we report two highly emissive COFs (TAT-COF and TPB-COF, Scheme 1) and the direct correlation of the structure with their

## Scheme 1. Synthesis Scheme of TAT-COF and TPB-COF



light absorption, charge transfer (CT), and luminescent properties. TAT-COF and TPB-COF were synthesized by the reaction of 2,4,6-trimethyl-1,3,5-triazine (TMTA) with star-shaped monomers, 2,7,12-triformyl-5,10,15-triethyltriindole (TAT) and 1,3,5-tris(4- formylphenyl)benzene (TFPB), respectively, via a Knoevenagel condensation reaction (Scheme 1). We hypothesize that fine tuning of the monomer structure in TAT with respect to TFPB alters the planarity, charge delocalization (conjugation), and  $\pi - \pi$  stacking (aggregation) of the COF structure, which are anticipated to affect the photophysical properties. Using the combination of experimental spectroscopic and computational studies, we not only show that the designed COFs can be used to generate white light but also identify how the physical structure of COFs can modulate CT, exciton relaxation, and emission quantum efficiency.

## ■ RESULTS AND DISCUSSION

The details of the synthetic procedure of TAT-COF and TPB-COF are described in the Supporting Information and follow the same procedure for TPB-COF reported previously. <sup>27,41</sup> The formation of both COFs was confirmed by FT-IR spectra, X-ray diffraction (XRD), scanning electron microscopy (SEM), and diffuse reflectance (DR) and emission spectra. The FT-IR spectra of TAT-COF (Figure 1a) and TPB-COF (Figure 1b) show the absence of the aldehyde band (1689 cm<sup>-1</sup>) that was present in TAT (Figure 1a) and the TFPB (Figure 1b) ligand and the presence of the characteristic vibrational stretching modes of a C=C trans configuration at 1630 and 978 cm<sup>-1</sup>, suggesting the complete condensation of

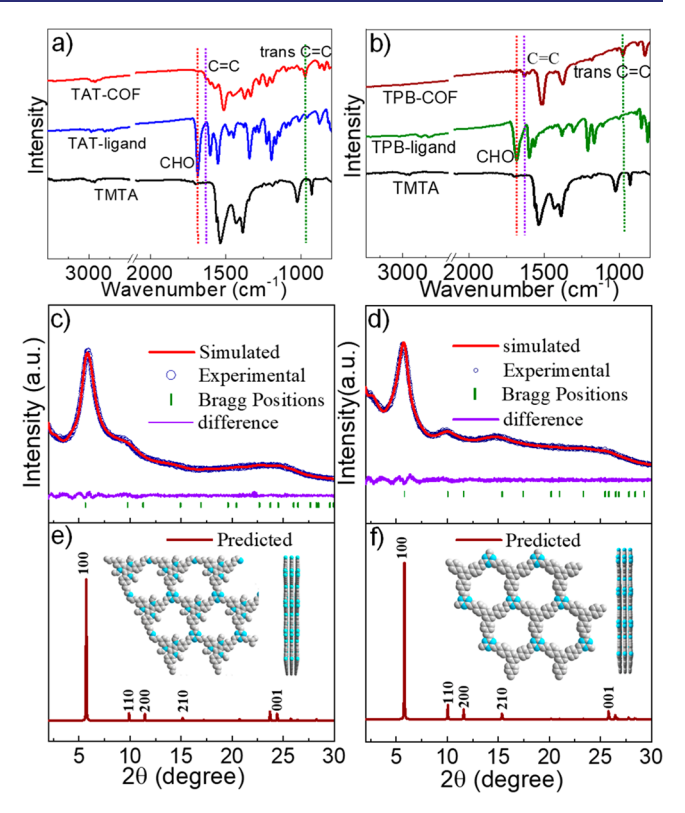


Figure 1. FT-IR spectra of (a) TAT-COF and (b) TPB-COF with the corresponding monomers. Powder XRD patterns of (c) TAT-COF and (d) TPB-COF: Pawley refinement of COFs (AA stacking) against the experimental data, the Bragg positions (green bar), and the refinement differences (purple). Simulated XRD of (e) TAT-COF and (f) TPB-COF. Insets give the top and side views of the structure modeling of TAT-COF and TPB-COF with AA stacking.

the starting monomers to form the olefin linkages in both COFs. The XRD pattern of TAT-COF (Figure 1c) shows peaks at 5.8, 9.8, 11.3, 14.9, and 24.4°, and that of TPB-COF (Figure 1d) shows distinguished peaks at 5.8, 10.1, 11.6, 15.4, and 25.8°, which can be assigned to (100), (110), (200), (210), and (001) facets (Figure 1e,f), respectively. A Pawley refinement of the eclipsed (AA) stacking mode (inset of Figure 1e,f and Table S1) modeled using Materials Studio yields XRD patterns (red plot in Figure 1c,d) that show negligible difference from the experimental data. In contrast, a staggered (AB) mode cannot reproduce the experimental XRD patterns, suggesting that the condensation reaction of monomers leads to the formation of TAT-COF and TPB-COF with an AA stacking mode.

The permanent porosity was investigated by N<sub>2</sub> sorption measurements at 77 K. As illustrated in Figure S1, the Brunauer–Emmett–Teller (BET) surface area of TPB-COF is 703 m²/g, which is comparable to the results reported previously. In contrast, the BET surface area of TAT-COF is only 91 m²/g. The low surface area of TAT-COF can be attributed to the ultramicroporous pores resulting from the bulky ethyl group. This is further supported by the type II isotherms, which indicate their low-porosity nature. Unlike TAT-COF, TPB-COF shows type I reversible isotherms, implying mesoporous characteristics. More importantly, both TAT-COF and TPB-COF show good thermal and chemical stability, as indicated by the TGA measurements (Figure S2) and the negligible change in position and intensity of XRD

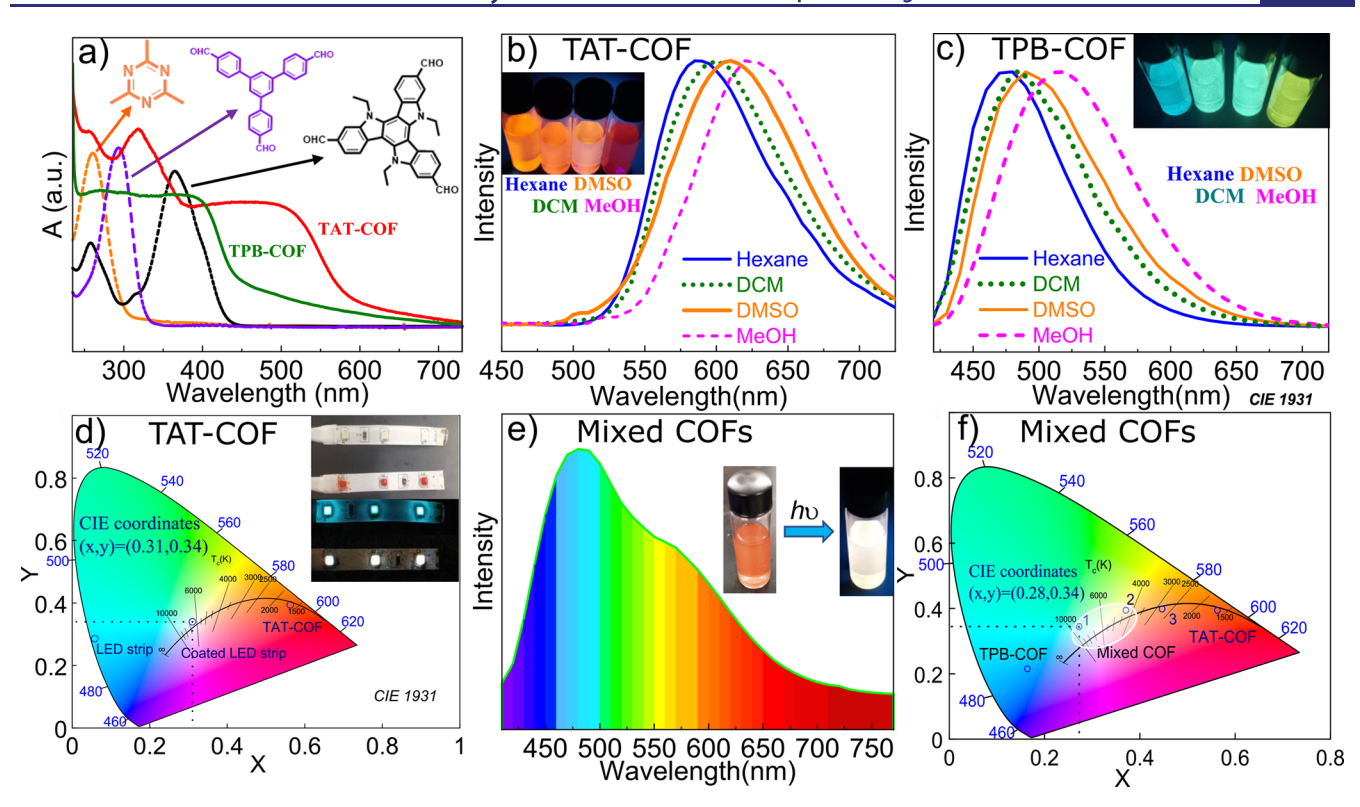


Figure 2. (a) Diffuse reflectance UV—visible spectra of TAT-COF and TPB-COF with those of the corresponding monomers. Emission spectra of (b) TAT-COF and (c) TPB-COF in hexane, DCM, DMSO, and MeOH. The insets show photographs of TAT-COF and TPB-COF suspensions in different solvents under UV light (365 nm). (d) CIE-1931 diagram and the positions of the coated LED strip, TAT-COF, and the LED strip. Insets give photographs of the LEDs. (e) Emission spectrum of mixed a TAT-COF and TPB-COF suspension. Insets give photographs of suspensions with and without UV light. (f) CIE-1931 coordinates and a CCT diagram for mixed COF suspensions with different ratios.

patterns after dispersedion in DMF, MeOH, hexane, water, HCl (12 M), and NaOH (12 M) solutions for 1 week (Figure S3). An SEM image of TAT-COF (Figure S4a) shows a fibrillar shape with a diameter of approximately 1  $\mu$ m and length of 10  $\mu$ m, while TPB-COF (Figure S4b) shows a morphology of spherical aggregates 1  $\mu$ m in diameter.

The formation of the COF structure was further supported by the DR and photoluminescence (PL) spectra. In comparison to their corresponding monomers, the DR spectra of both COFs (Figure 2a) exhibit extended absorption in the visible region, which can be attributed to a CT transition arising from the donor–acceptor pairs via  $\pi$ -conjugation in the skeleton and/or interlayer stacking. The emission spectra of TAT-COF and TPB-COF (Figure S5) after 400 nm excitation show a distinct emission band with a significant red shift with respect to their single units, implying that the CT transition is responsible for the emission of COFs. In addition, the emission spectra of both samples show a strong dependence on solvent polarity. When TAT-COF was dispersed in hexane, orange light was emitted at 575 nm (Figure 2b). When more polar solvents were used, for which the solvent polarity increases in the order of DCM < DMSO < MeOH, the emission maxima shift to longer wavelength (from orange to red). A similar trend of bathochromic shift with increasing solvent polarity was observed in the emission spectrum of TPB-COF (Figure 2c), indicating the polar nature of the CT state of the COFs. Along with the bathochromic shift, the PL quantum yields (PLQYs) of the two COFs are also sensitive to the environment. As shown in Table S2, a PLQY value of 17.82% was observed for TAT-COF in DCM and decreased to 5.29% and 2% in DMSO and MeOH, respectively. In

comparison to TAT-COF, TPB-COF exhibits much stronger emission with a PLQY of up to 62.17% in DCM. The different PLQYs of TAT-COF and TPB-COF are correlated to the difference in transition dipole moment orientation and the geometrical effect of the framework, which will be discussed later.

The tunable emission color as well as the high PLQY of TAT-COFs and TPB-COFs make them of interest in optical applications such as white-light-emitting diodes (WLEDs). RGB (red, green, blue) methods and phosphor methods are two conventional approaches to produce white light with LEDs by the proper mixture of LEDs with three primary colors (blue, green, red) or the combination of a blue LED with a yellow phosphor coating. 42 As white light can be generated by mixing two complementary colors, we then explored the possibility to use TAT-COF for WLEDs. As shown in Figure 2d, white light was obtained by simply coating TAT-COF on the surface of a cyan LED strip (~485 nm). The CIE coordinates were determined to be (0.31, 0.34) and found to be cold white (CCT 6500K). More interestingly, white light with variable temperature can be easily obtained by mixing the two COFs in certain ratios. Shown in Figure 2e is the emission spectrum of the mixed TAT-COF and TPB-COF dispersion in DCM with a ratio of 3.5:1, which covers the entire visible spectrum. Upon illumination of the mixed suspension by UV light (365 nm), white light emission is clearly visible, as shown in the inset of Figure 2e. The CIE coordinates of the mixed COFs (Figure 2f) were determined to be (0.28, 0.34), resulting in cold white

To gain insight into the origin of the observed emission behaviors of these COFs, we first measured the excited state (ES) lifetime of TAT-COF and TPB-COF by time-resolved emission spectroscopy after 400 nm excitation. Figure 3a

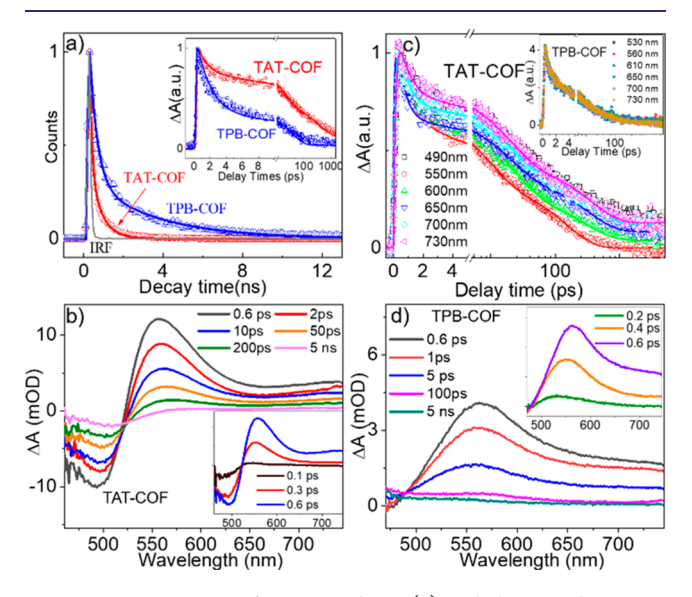


**Figure 3.** Comparison of emission decay (a) and electron absorption decay (inset) between TAT-COF and TPB-COF. Transient absorption spectra of TAT-COF (b) and TPB-COF (d) following 400 nm excitation. (c) Comparison of TA kinetics of TAT-COF and TPB-COF (inset) at different wavelengths. The solid lines are the fits to the kinetic traces.

compares the emission decays of TAT-COF and TPB-COF collected at 580 and 450 nm, respectively, corresponding to their CT emissions. The emission decay is much faster in TAT-COF than in TPB-COF, suggesting that the CT state in the former has a shorter emission lifetime than the latter, which is consistent with its lower PLQY and suggests a "nonfluorescent J-type" aggregation behavior, as supported by timedependent density functional theory (TDDFT, discussed later).43 Each decay curve can be fit by a biexponential function, from which we obtained the amplitude weighted lifetimes, which are 0.24 and 1.2 ns for TAT-COF and TPB-COF (Table S3), respectively. In addition to emission lifetime, we also examined the ES dynamics of these COFs using femtosecond transient absorption (TA) spectroscopy, which allowed us to probe the early time dynamics that cannot be resolved by time-resolved emission spectroscopy. Figure 3b shows the TA spectra of TAT-COF following 400 nm excitation. Immediately following the excitation, the TA spectra of TAT-COF show the formation of a negative feature centered around 500 nm and a broad positive absorption band from 525 nm to the red end of our spectral window (inset of Figure 3b). The negative feature can be assigned to an exciton bleaching (EB) band due to the occupation of the conduction band (CB) by electrons following photoexcitation. The positive band can be attributed to the CB electron absorption in the framework. The formation of both EB and electron absorption bands show a rising component within ~600 fs, which can be attributed to the relaxation of the electrons from the high- to low-energy CB. As shown in Figure 3c, the electron absorption of TAT-COF at 560 nm is found to decay more quickly with respect to the longer wavelength region. A similar probe wavelength dependent kinetics has been previously reported in other solid-state materials and is likely associated with the presence of a trap state.<sup>44</sup> Similar spectral

features, i.e. negative EB and positive electron absorption (increases within 600 fs) were observed for TPB-COF (Figure 3d), although the negative band of TPB-COF is barely seen because of the limit of our TA window. Unlike TAT-COF, the kinetic traces for electron absorption at different probe wavelengths appear to be same for TPB-COF (inset of Figure 3c), suggesting exciton relaxation dynamics different from those of TAT-COF. More interestingly, we note that the electron absorption kinetics of TPB-COF exhibits faster decay in comparison to TAT-COF (inset of Figure 3a), which conflicts with the time-resolved emission results, where its emission lifetime is longer in comparison to that of TAT-COF (Figure 3a). This conflict further supports that different exciton relaxation pathways are involved in these COFs.

To uncover the origins that result in distinct exciton relaxation dynamics in TAT-COF and TPB-COF, we turned to TDDFT (procedure outlined in the Supporting Information) to examine the direct correlation of the optical properties of the COFs with their topology, structure, and composition, as these structural parameters are all expected to play a role in the photophysical properties of COFs. We prefix the computational work by acknowledging that, although COFs polymerize into extended structures, the size of the systems that can be studied by TDDFT are limited by computational expense. As such, we decomposed the extended COF structures into smaller units as a tradeoff for reasonable timeliness and efficiency. The unit selection, however, is critical to ensure meaningful insights. In this work, the region including one triazine ring and one of either TAT or TPB is selected as the unit for study (Figure 4a,b), and the rationale for this selection is discussed in the Supporting Information. Finally, COFs readily form aggregated structures, which is especially important, as our physical experiments herein are conducted in the condensed phase. To account for aggregation, TDDFT

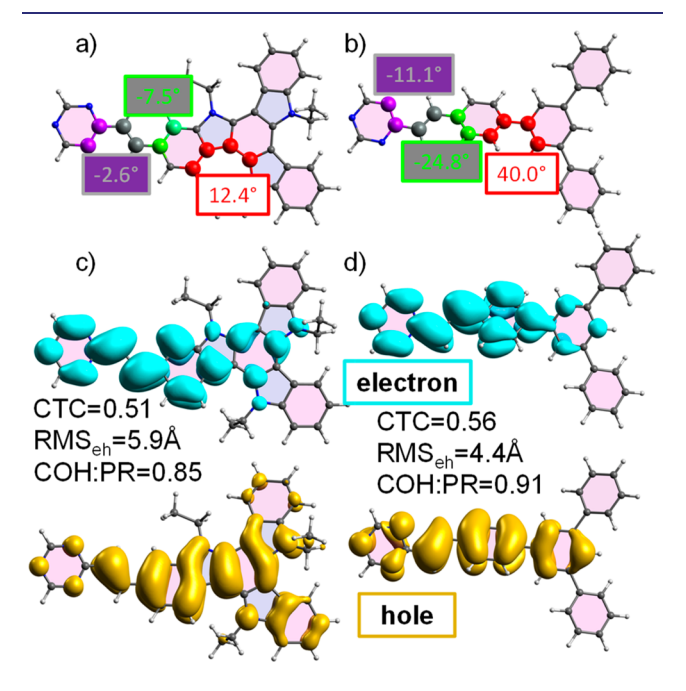


**Figure 4.** Representative units selected for TDDFT study including important dihedral angles of (a) TAT-COF and (b) TPB-COF. Dihedrals in TPB-COF are larger than those in TAT-COF, demonstrating the difference in planarity. Natural transition orbitals and quantitative CT measures of (c) TAT-COF and (d) TPB-COF.

is used to study not only single layers of COF but also the interlayer interactions between multiple layers (one to three) of our small units.

TDDFT is first used to examine the nature of electronic transitions of TAT-COF and TPB-COF. The predicted transitions indicate TAT-COF possesses lower energy absorption and oscillator strength in comparison to TPB-COF (Table S5), which directly reflects the DR spectrum above and suggests the validity of our computational model. The natural transition orbitals (NTOs) of the predicted electronic transitions indicate that the planarity of TAT-COF (Figure 4a,c) allows for significant delocalization. This is in contrast with the propeller-like structure of TPB-COF (Figure 4b,d) that prevents a similar delocalization. In addition, branches of TPB are arranged meta to one another around the benzene core, which is inconducive with their ortho/para electron directing nature. 45 This meta arrangement, along with the twisted propeller structure, prevents conjugation across the TPB monomer. On the other hand, TAT-COF possesses indole units which are directly attached to a shared benzene core, thus allowing for more conjugation and lower energy electronic transitions in comparison to TPB-COF. These results agree well with the DR and emission spectra of COFs, where TAT-COF shows significantly red shifted absorption/ emission, suggesting that in-plane conjugation plays an important role in extending the light absorption/emission properties of COFs into the visible region.

In addition to conjugation, CT and the effect of aggregation on the electronic structure needs to be considered in order to have a complete picture of the correlation of the COF structure with its light absorption properties. Before undertaking a complete discussion of interlayer interactions, we must first lay out a few quantitative CT measures. Through analysis of the transition density matrix (TDM, details outlined in the Supporting Information), 46-49 we gain a quantitative value for the CT character (CTC). Due to the difficulties in using CTC to describe the intermediate cases of CT, 50,51 we also evaluated electron-hole separation (COH:PR) and exciton size (RMS<sub>eh</sub>) as additional measures for CT characteristics (Figure 4c,d and Table S6). In comparison to TPB-COF, TAT-COF has less intralayer CTC and COH:PR but a larger overall exciton, which is due to the greater degree of electron delocalization in the ground state (GS) as shown in the NTOs (Figure 4). After aggregation to three layers, CTC does not change, but COH:PR decreases, and RMSeh increases by 3% (Table S6). Furthermore, the transition energy decreases by 0.01 eV with an increase in oscillator strength by 0.2 au. On the other hand, TPB-COF experiences a small increase of intralayer COH:PR and a 7% increase in RMS<sub>eh</sub> (Table S6), corresponding with an increase in the transition energy by 0.1 eV and in the oscillator strength by more than 1 au. These results suggest that TPB-COF exhibits more intralayer CT enhancement on aggregation, as indicated by the growth of its exciton.

To uncover why the exciton in TPB-COF grows and gains oscillator strength upon aggregation, we need to have an indepth understanding of the exciton interactions,  $^{52}$  for which the structure, excited-state polarizability,  $^{53-57}$  and superexchange CT coupling need to be considered. First, it is important to note that TAT-COF and TPB-COF are predicted to have distinctly different aggregate structures. TAT-COF (Figure 5a) is offset in the x direction by 2.32 Å and in the y direction by -2.95 Å, while TPB-COF (Figure 5b) is offset

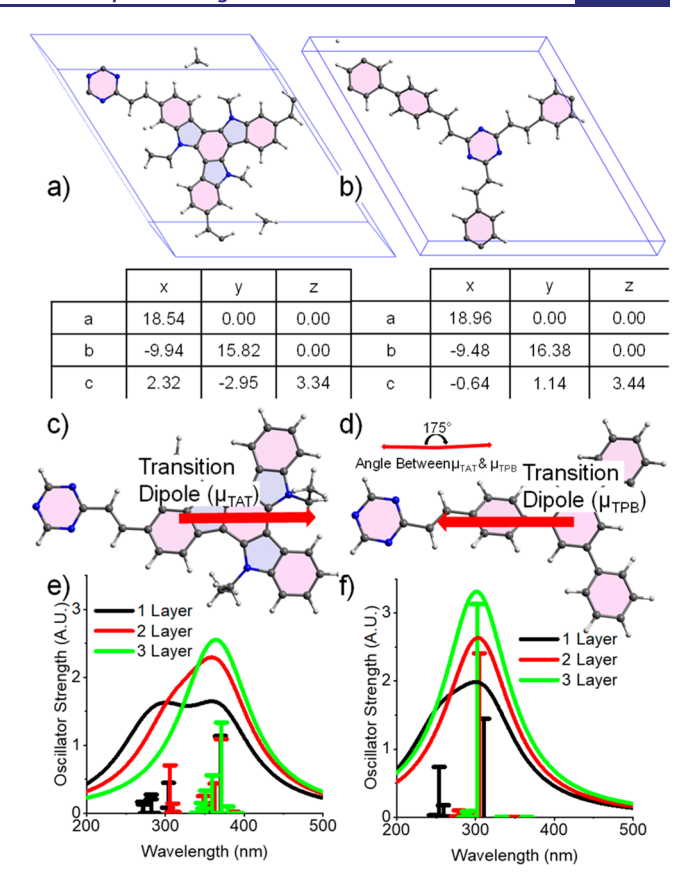


**Figure 5.** Interlayer arrangements of (a) TAT-COF and (b) TPB-COF obtained from DFTB structure optimization. TDDFT-predicted transition dipole moments of (c) TAT-COF and (d) TPB-COF. The structures were placed into a reference frame so that their transition dipole moments could be easily compared. The TDDFT predicted absorption spectra upon aggregation of (e) TAT-COF and (f) TPB-COF.

-0.64 Å in the x direction and 1.14 Å in the y direction. Simulated PXRD patterns of the COF structures show reasonably good agreement with the experimental patterns (Figure S7), although we acknowledge that bulk COFs may assume various stacking patterns. As such, we assume our converged structures yield plausible realistic representations. Nonetheless, the stacking geometries generally approach "card pack" and should lead to "H-type" aggregates, although TAT-COF may be more of an intermediate case within Kasha's model of the exciton. 52 However, since the transition energy of TAT-COF decreases with aggregation, we must consider other competing effects (Table S5). With regard to the ES polarizability, both COFs undergo transitions with dipole moments of a similar magnitude, but they have opposing orientations, making a 175° angle (Figure 5). This observation reveals that the orientation of the transition dipole moment in TAT-COF opposes the direction of the intramolecular CT. Thus, the transition dipole moment interacts to stabilize the polarizable CT state, which prevents aggregation-induced CT enhancement and lowers the oscillation strength of transitions in comparison to TPB-COF (Figure 5e,f). Overall, this also narrows the exciton bandwidth between the bright transition and the lowest dark transition (0.17 eV), red-shifts the absorption, and suggests that TAT-COF may belong to the "non-fluorescent J-type" class of aggregates. 59 In contrast, the opposite can be seen in the results for TPB-COF aggregatesaggregation-induced CT enhancement is expected, the oscillator strength increases significantly (Figure 5f), and the exciton bandwidth is significantly widened (0.71 eV), leading to an assignment as a traditional "H-type" aggregate. Superexchange CT coupling is the last piece to consider and can be gauged by the same CT measures above, but in the interlayer direction. For the two-layer system, TAT-COF has almost 5 times as much CTC and ~35% more COH:PR in comparison to TPB-COF (Table S6). Notably, COH:PR of TAT-COF approaches 1 (0.73), which suggests that there is strong mixing of Frenkel and CT states. For three layers, this quantity is tempered somewhat, as COH:PR decreases to 0.55 but is still 45% greater than that for the three-layer TPB-COF system. Evidence provided by the electron density map (Figure S8) indicates interaction between two of the three TAT-COF layers in the off-diagonal elements, whereas TPB-COF mainly incorporates interaction localized on each layer in the ondiagonal elements. Overall, these results suggest that the fused, planar structure of TAT-COF yields more interlayer CT mixed into allowed transitions in comparison to TPB-COF.

Combining the computational results with the fundamental spectroscopic data above provides a robust explanation for experimental differences between exciton formation and relaxation dynamics in TPB-COF and TAT-COF. These comparative experimental observations in TAT-COF are (a) red shifting of the absorption spectrum, (b) slower TA decay kinetics, (c) probe-dependent TA decay kinetics, (d) shorter emission lifetime, and (e) lower PLQY. Delocalization and the CT stabilizing orientation of the transition dipole moment in TAT-COF contribute to the red shift in the absorption spectrum. In turn, this narrows the exciton bandwidth and shortens the internal conversion channel. As shown in the model we propose to illustrate these experimental and computational results (Figure 6), the photoexcitation of

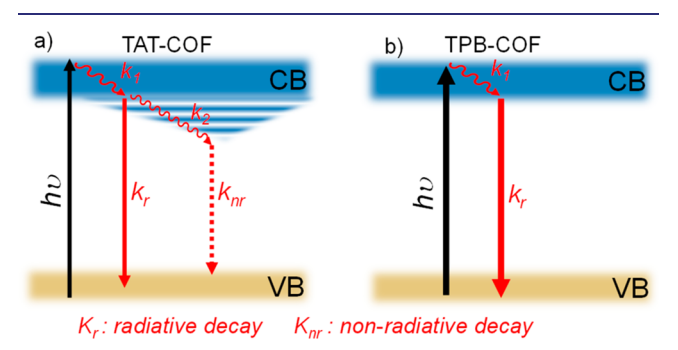


Figure 6. Energy diagrams of TAT-COF (a) and TPB-COF (b) that illustrate exciton relaxation dynamics.

COFs promotes the electrons from their valence band (VB) to the high-energy level of the CB, which then quickly relax down to the edge of the CB, corresponding to the increasing component within 600 fs  $(k_1)$ . Due to the presence of trap states in TAT-COF, some electrons relax down to this trap state  $(k_2)$ , which is responsible for the probe-dependent kinetics observed in the TA spectra of TAT-COF. Because the electrons in trap states typically have longer lifetimes, which coincides with the shortened internal conversion in TAT-COF, this yields the appearance of slower electron absorption decay in TAT-COF than in TPB-COF, where the latter undergoes more internal conversion and barely populates trap states and thus shows a negligible dependence of kinetic traces on probe wavelength. The trap state is a nonradiative state, which well

explains that TPB-COF has a much longer emission lifetime and higher PLQY than TAT-COF, as time-resolved emission spectroscopy only measures the emissive ES. While the origin of the trap state remains unclear, one possibility could arise from excimer formation, 60 which has also been recently reported to lead to probe-dependent TA kinetics in COF-5. However, further TA experiments using a near-IR probe do not show the spectral features of an excimer (Figure S9), which may suggest that the trap state herein may result from other factors rather than the formation of an excimer.

#### CONCLUSIONS

In summary, we report the synthesis, white-light emission, and direct correlation of the structure (conjugation and aggregation) with the light-harvesting, CT, and ES dynamics of two conjugated sp<sup>2</sup>-C-COFs with embedded donor—acceptor pairs. We show that both COFs are highly emissive, where white light can be obtained by simply coating the COFs on an LED strip. On adjustment of the ratio of TAT-COF and TPB-COF in solution, the mixed COFs exhibit different colors across the visible spectrum. Using the combination of time-resolved absorption and emission spectroscopy as well as TDDFT calculations, we show that the planar backbone of TAT-COF facilitates in-plane charge delocalization, resulting in a broader absorption in the visible region with respect to TPB-COF. The transition dipoles interact with polarizable intramolecular CT states to narrow or widen the exciton bandwidth, leading to shorter and longer internal conversions in TAT-COF and TPB-COF, respectively. In addition, TAT-COF with a planar backbone exhibits stronger interlayer CT in comparison to TPB-COF with propeller-like monomers, which suppresses the fluorescence quantum yield. These results not only demonstrate the great potential of COFs as organic luminescent materials but also provide unprecedented insight into how the COF structure (conjugation and aggregation) should be considered for the rational design of highly emissive COFs.

## ASSOCIATED CONTENT

## **Supporting Information**

The Supporting Information is available free of charge at https://pubs.acs.org/doi/10.1021/jacs.0c11719.

Details of synthetic and computational calculation procedures,  $N_2$  adsorption and desorption isotherms, TGA, XRD patterns, a comparison of DR spectra with TDDFT calculations, emission spectra, excitation spectra, electron density maps, fitting parameters, and TDDFT results (PDF)

## AUTHOR INFORMATION

## **Corresponding Author**

Jier Huang — Department of Chemistry, Marquette University, Milwaukee, Wisconsin 53201, United States; orcid.org/0000-0002-2885-5786; Email: jier.huang@marquette.edu

#### **Authors**

Sizhuo Yang — Department of Chemistry, Marquette
University, Milwaukee, Wisconsin 53201, United States
Daniel Streater — Department of Chemistry, Marquette
University, Milwaukee, Wisconsin 53201, United States
Christian Fiankor — Department of Chemistry, University of
Nebraska-Lincoln, Lincoln, Nebraska 68588, United States

Jian Zhang — Department of Chemistry, University of Nebraska-Lincoln, Lincoln, Nebraska 68588, United States; orcid.org/0000-0003-0274-0814

Complete contact information is available at: https://pubs.acs.org/10.1021/jacs.0c11719

#### **Author Contributions**

§S.Y. and D.S. contributed equally.

#### Notes

The authors declare no competing financial interest.

### ACKNOWLEDGMENTS

This research was supported by the U.S. Department of Energy, Office of Science, Office of Basic Energy Sciences, under Award No. DE-SC0020122. Use of the femtosecond-NIR transient absorption spectrometer at the Center for Nanoscale Materials in Argonne National Laboratory was supported by the U.S. Department of Energy, Office of Science, Office of Basic Energy Sciences, under award no. DE-AC02-06CH11357. We thank Dr. David Gosztola and Dr. Gary Wiederrecht at the CNM for collecting NIR TA data. We acknowledge support from National Science Foundation award CNS-1828649 "MRI: Acquisition of iMARC: High Performance Computing for STEM Research and Education in Southeast Wisconsin".

### REFERENCES

- (1) Grimsdale, A. C.; Leok Chan, K.; Martin, R. E.; Jokisz, P. G.; Holmes, A. B. Synthesis of Light-Emitting Conjugated Polymers for Applications in Electroluminescent Devices. *Chem. Rev.* **2009**, *109* (3), 897–1091.
- (2) Lamansky, S.; Djurovich, P.; Murphy, D.; Abdel-Razzaq, F.; Lee, H.-E.; Adachi, C.; Burrows, P. E.; Forrest, S. R.; Thompson, M. E. Highly Phosphorescent Bis-Cyclometalated Iridium Complexes: Synthesis, Photophysical Characterization, and Use in Organic Light Emitting Diodes. J. Am. Chem. Soc. 2001, 123 (18), 4304–4312.
- (3) Tang, C. W.; VanSlyke, S. A. Organic electroluminescent diodes. *Appl. Phys. Lett.* **1987**, *51* (12), 913–915.
- (4) Zhang, S.-W.; Swager, T. M. Fluorescent Detection of Chemical Warfare Agents: Functional Group Specific Ratiometric Chemosensors. *J. Am. Chem. Soc.* **2003**, *125* (12), 3420–3421.
- (5) Basabe-Desmonts, L.; Reinhoudt, D. N.; Crego-Calama, M. Design of fluorescent materials for chemical sensing. *Chem. Soc. Rev.* **2007**, *36* (6), 993–1017.
- (6) Sinkeldam, R. W.; Greco, N. J.; Tor, Y. Fluorescent Analogs of Biomolecular Building Blocks: Design, Properties, and Applications. *Chem. Rev.* **2010**, *110* (5), 2579–2619.
- (7) Niu, G.; Zhang, R.; Kwong, J. P. C.; Lam, J. W. Y.; Chen, C.; Wang, J.; Chen, Y.; Feng, X.; Kwok, R. T. K.; Sung, H. H. Y.; Williams, I. D.; Elsegood, M. R. J.; Qu, J.; Ma, C.; Wong, K. S.; Yu, X.; Tang, B. Z. Specific Two-Photon Imaging of Live Cellular and Deep-Tissue Lipid Droplets by Lipophilic AlEgens at Ultralow Concentration. *Chem. Mater.* **2018**, *30* (14), 4778–4787.
- (8) Ostroverkhova, O. Organic Optoelectronic Materials: Mechanisms and Applications. *Chem. Rev.* **2016**, *116* (22), 13279–13412.
- (9) Salehi, A.; Fu, X. Y.; Shin, D. H.; So, F. Recent Advances in OLED Optical Design. Adv. Funct. Mater. 2019, 29 (15), 1808803.
- (10) Wei, Q.; Potzsch, R.; Liu, X. L.; Komber, H.; Kiriy, A.; Voit, B.; Will, P. A.; Lenk, S.; Reineke, S. Hyperbranched Polymers with High Transparency and Inherent High Refractive Index for Application in Organic Light-Emitting Diodes. *Adv. Funct. Mater.* **2016**, *26* (15), 2545–2553.
- (11) Jones, B. A.; Facchetti, A.; Wasielewski, M. R.; Marks, T. J. Tuning Orbital Energetics in Arylene Diimide Semiconductors. Materials Design for Ambient Stability of n-Type Charge Transport. J. Am. Chem. Soc. 2007, 129 (49), 15259–15278.

- (12) Zheng, Q.; Juette, M. F.; Jockusch, S.; Wasserman, M. R.; Zhou, Z.; Altman, R. B.; Blanchard, S. C. Ultra-stable organic fluorophores for single-molecule research. *Chem. Soc. Rev.* **2014**, *43* (4), 1044–1056.
- (13) Wu, D.; Sedgwick, A. C.; Gunnlaugsson, T.; Akkaya, E. U.; Yoon, J.; James, T. D. Fluorescent chemosensors: the past, present and future. *Chem. Soc. Rev.* **2017**, *46* (23), 7105–7123.
- (14) Uoyama, H.; Goushi, K.; Shizu, K.; Nomura, H.; Adachi, C. Highly efficient organic light-emitting diodes from delayed fluorescence. *Nature* **2012**, 492 (7428), 234–238.
- (15) Luo, J.; Xie, Z.; Lam, J. W. Y.; Cheng, L.; Chen, H.; Qiu, C.; Kwok, H. S.; Zhan, X.; Liu, Y.; Zhu, D.; Tang, B. Z. Aggregation-induced emission of 1-methyl-1,2,3,4,5-pentaphenylsilole. *Chem. Commun.* 2001, No. 18, 1740–1741.
- (16) Mei, J.; Leung, N. L. C.; Kwok, R. T. K.; Lam, J. W. Y.; Tang, B. Z. Aggregation-Induced Emission: Together We Shine, United We Soar! *Chem. Rev.* **2015**, *115* (21), 11718–11940.
- (17) Zhao, Z.; Zhang, H.; Lam, J. W. Y.; Tang, B. Z. Aggregation-Induced Emission: New Vistas at the Aggregate Level. *Angew. Chem., Int. Ed.* **2020**, *59*, 9888.
- (18) Dalapati, S.; Gu, C.; Jiang, D. Luminescent Porous Polymers Based on Aggregation-Induced Mechanism: Design, Synthesis and Functions. *Small* **2016**, *12* (47), 6513–6527.
- (19) Diercks, C. S.; Yaghi, O. M. The atom, the molecule, and the covalent organic framework. *Science* **2017**, 355 (6328), No. eaal1585.
- (20) Geng, K.; He, T.; Liu, R.; Dalapati, S.; Tan, K. T.; Li, Z.; Tao, S.; Gong, Y.; Jiang, Q.; Jiang, D. Covalent Organic Frameworks: Design, Synthesis, and Functions. *Chem. Rev.* **2020**, *120* (16), 8814–8933
- (21) Chen, X.; Geng, K.; Liu, R.; Tan, K. T.; Gong, Y.; Li, Z.; Tao, S.; Jiang, Q.; Jiang, D. Covalent Organic Frameworks: Chemical Approaches to Designer Structures and Built-In Functions. *Angew. Chem., Int. Ed.* **2020**, *59* (13), 5050–5091.
- (22) Ding, S.-Y.; Wang, W. Covalent organic frameworks (COFs): from design to applications. *Chem. Soc. Rev.* **2013**, 42 (2), 548–568.
- (23) Lohse, M. S.; Bein, T. Covalent Organic Frameworks: Structures, Synthesis, and Applications. *Adv. Funct. Mater.* **2018**, 28 (33), 1705553.
- (24) Haldar, S.; Chakraborty, D.; Roy, B.; Banappanavar, G.; Rinku, K.; Mullangi, D.; Hazra, P.; Kabra, D.; Vaidhyanathan, R. Anthracene-Resorcinol Derived Covalent Organic Framework as Flexible White Light Emitter. *J. Am. Chem. Soc.* **2018**, *140* (41), 13367–13374.
- (25) Haug, W. K.; Moscarello, E. M.; Wolfson, E. R.; McGrier, P. L. The luminescent and photophysical properties of covalent organic frameworks. *Chem. Soc. Rev.* **2020**, 49 (3), 839–864.
- (26) Wang, X.; Chen, L.; Chong, S. Y.; Little, M. A.; Wu, Y.; Zhu, W.-H.; Clowes, R.; Yan, Y.; Zwijnenburg, M. A.; Sprick, R. S.; Cooper, A. I. Sulfone-containing covalent organic frameworks for photocatalytic hydrogen evolution from water. *Nat. Chem.* **2018**, *10* (12), 1180–1189.
- (27) Wei, S.; Zhang, F.; Zhang, W.; Qiang, P.; Yu, K.; Fu, X.; Wu, D.; Bi, S.; Zhang, F. Semiconducting 2D Triazine-Cored Covalent Organic Frameworks with Unsubstituted Olefin Linkages. *J. Am. Chem. Soc.* **2019**, *141* (36), 14272–14279.
- (28) Wan, S.; Guo, J.; Kim, J.; Ihee, H.; Jiang, D. A Belt-Shaped, Blue Luminescent, and Semiconducting Covalent Organic Framework. *Angew. Chem., Int. Ed.* **2008**, *47* (46), 8826–8830.
- (29) Wan, S.; Guo, J.; Kim, J.; Ihee, H.; Jiang, D. A Photoconductive Covalent Organic Framework: Self-Condensed Arene Cubes Composed of Eclipsed 2D Polypyrene Sheets for Photocurrent Generation. *Angew. Chem., Int. Ed.* **2009**, 48 (30), 5439–5442.
- (30) Dalapati, S.; Jin, S.; Gao, J.; Xu, Y.; Nagai, A.; Jiang, D. An Azine-Linked Covalent Organic Framework. J. Am. Chem. Soc. 2013, 135 (46), 17310–17313.
- (31) Auras, F.; Ascherl, L.; Hakimioun, A. H.; Margraf, J. T.; Hanusch, F. C.; Reuter, S.; Bessinger, D.; Döblinger, M.; Hettstedt, C.; Karaghiosoff, K.; Herbert, S.; Knochel, P.; Clark, T.; Bein, T. Synchronized Offset Stacking: A Concept for Growing Large-Domain

- and Highly Crystalline 2D Covalent Organic Frameworks. J. Am. Chem. Soc. 2016, 138 (51), 16703–16710.
- (32) Crowe, J. W.; Baldwin, L. A.; McGrier, P. L. Luminescent Covalent Organic Frameworks Containing a Homogeneous and Heterogeneous Distribution of Dehydrobenzoannulene Vertex Units. *J. Am. Chem. Soc.* **2016**, *138* (32), 10120–10123.
- (33) Evans, A. M.; Castano, I.; Brumberg, A.; Parent, L. R.; Corcos, A. R.; Li, R. L.; Flanders, N. C.; Gosztola, D. J.; Gianneschi, N. C.; Schaller, R. D.; Dichtel, W. R. Emissive Single-Crystalline Boroxine-Linked Colloidal Covalent Organic Frameworks. *J. Am. Chem. Soc.* **2019**, *141* (50), 19728–19735.
- (34) Li, X.; Gao, Q.; Wang, J.; Chen, Y.; Chen, Z.-H.; Xu, H.-S.; Tang, W.; Leng, K.; Ning, G.-H.; Wu, J.; Xu, Q.-H.; Quek, S. Y.; Lu, Y.; Loh, K. P. Tuneable near white-emissive two-dimensional covalent organic frameworks. *Nat. Commun.* **2018**, 9 (1), 2335.
- (35) Dong, J.; Li, X.; Peh, S. B.; Yuan, Y. D.; Wang, Y.; Ji, D.; Peng, S.; Liu, G.; Ying, S.; Yuan, D.; Jiang, J.; Ramakrishna, S.; Zhao, D. Restriction of Molecular Rotors in Ultrathin Two-Dimensional Covalent Organic Framework Nanosheets for Sensing Signal Amplification. *Chem. Mater.* **2019**, *31* (1), 146–160.
- (36) Zhou, T.-Y.; Xu, S.-Q.; Wen, Q.; Pang, Z.-F.; Zhao, X. One-Step Construction of Two Different Kinds of Pores in a 2D Covalent Organic Framework. *J. Am. Chem. Soc.* **2014**, *136* (45), 15885–15888.
- (37) Dalapati, S.; Jin, E.; Addicoat, M.; Heine, T.; Jiang, D. Highly Emissive Covalent Organic Frameworks. *J. Am. Chem. Soc.* **2016**, *138* (18), 5797–5800.
- (38) Ding, H.; Li, J.; Xie, G.; Lin, G.; Chen, R.; Peng, Z.; Yang, C.; Wang, B.; Sun, J.; Wang, C. An AIEgen-based 3D covalent organic framework for white light-emitting diodes. *Nat. Commun.* **2018**, *9* (1), 5234
- (39) Jin, E.; Li, J.; Geng, K.; Jiang, Q.; Xu, H.; Xu, Q.; Jiang, D. Designed synthesis of stable light-emitting two-dimensional sp2 carbon-conjugated covalent organic frameworks. *Nat. Commun.* **2018**, 9 (1), 4143.
- (40) Jadhav, T.; Fang, Y.; Patterson, W.; Liu, C.-H.; Hamzehpoor, E.; Perepichka, D. F. 2D Poly(arylene vinylene) Covalent Organic Frameworks via Aldol Condensation of Trimethyltriazine. *Angew. Chem., Int. Ed.* **2019**, 58 (39), 13753–13757.
- (41) Acharjya, A.; Pachfule, P.; Roeser, J.; Schmitt, F.-J.; Thomas, A. Vinylene-Linked Covalent Organic Frameworks by Base-Catalyzed Aldol Condensation. *Angew. Chem., Int. Ed.* **2019**, *58* (42), 14865–14870.
- (42) Pimputkar, S.; Speck, J. S.; DenBaars, S. P.; Nakamura, S. Prospects for LED lighting. *Nat. Photonics* **2009**, *3* (4), 180–182.
- (43) Ayari, S.; Smiri, A.; Hichri, A.; Jaziri, S.; Amand, T. Radiative lifetime of localized excitons in transition-metal dichalcogenides. *Phys. Rev. B: Condens. Matter Mater. Phys.* **2018**, 98 (20), 205430.
- (44) Ludwig, J.; An, L.; Pattengale, B.; Kong, Q.; Zhang, X.; Xi, P.; Huang, J. Ultrafast Hole Trapping and Relaxation Dynamics in p-Type CuS Nanodisks. *J. Phys. Chem. Lett.* **2015**, 6 (14), 2671–2675.
- (45) Thomas, S.; Li, H.; Zhong, C.; Matsumoto, M.; Dichtel, W. R.; Bredas, J.-L. Electronic Structure of Two-Dimensional  $\pi$ -Conjugated Covalent Organic Frameworks. *Chem. Mater.* **2019**, *31* (9), 3051–3065.
- (46) Li, Y.; Ullrich, C. A. Time-dependent transition density matrix. *Chem. Phys.* **2011**, 391 (1), 157–163.
- (47) Plasser, F.; Lischka, H. Analysis of Excitonic and Charge Transfer Interactions from Quantum Chemical Calculations. *J. Chem. Theory Comput.* **2012**, *8* (8), 2777–2789.
- (48) Plasser, F. TheoDORE: A toolbox for a detailed and automated analysis of electronic excited state computations. *J. Chem. Phys.* **2020**, 152 (8), 084108.
- (49) Bäppler, S. A.; Plasser, F.; Wormit, M.; Dreuw, A. Exciton analysis of many-body wave functions: Bridging the gap between the quasiparticle and molecular orbital pictures. *Phys. Rev. A: At., Mol., Opt. Phys.* **2014**, *90* (5), 052521.
- (50) Guido, C. A.; Cortona, P.; Mennucci, B.; Adamo, C. On the Metric of Charge Transfer Molecular Excitations: A Simple Chemical Descriptor. *J. Chem. Theory Comput.* **2013**, *9* (7), 3118–3126.

- (51) Moore, B.; Sun, H.; Govind, N.; Kowalski, K.; Autschbach, J. Charge-Transfer Versus Charge-Transfer-Like Excitations Revisited. *J. Chem. Theory Comput.* **2015**, *11* (7), 3305–3320.
- (52) Kasha, M. Energy Transfer Mechanisms and the Molecular Exciton Model for Molecular Aggregates. *Radiat. Res.* **1963**, 20 (1), 55–70.
- (53) Campioli, E.; Sanyal, S.; Marcelli, A.; Di Donato, M.; Blanchard-Desce, M.; Mongin, O.; Painelli, A.; Terenziani, F. Addressing Charge-Transfer and Locally-Excited States in a Twisted Biphenyl Push-Pull Chromophore. *ChemPhysChem* **2019**, 20 (21), 2860–2873.
- (54) Guasch, J.; Grisanti, L.; Souto, M.; Lloveras, V.; Vidal-Gancedo, J.; Ratera, I.; Painelli, A.; Rovira, C.; Veciana, J. Intra- and Intermolecular Charge Transfer in Aggregates of Tetrathiafulvalene-Triphenylmethyl Radical Derivatives in Solution. *J. Am. Chem. Soc.* **2013**, *135* (18), 6958–6967.
- (55) Painelli, A.; Terenziani, F. Multielectron Transfer in Clusters of Polar-Polarizable Chromophores. *J. Am. Chem. Soc.* **2003**, *125* (19), 5624–5625.
- (56) Zheng, C.; Zhong, C.; Collison, C. J.; Spano, F. C. Non-Kasha Behavior in Quadrupolar Dye Aggregates: The Red-Shifted H-Aggregate. *J. Phys. Chem. C* **2019**, *123* (5), 3203–3215.
- (57) Zhong, C.; Bialas, D.; Spano, F. C. Unusual Non-Kasha Photophysical Behavior of Aggregates of Push—Pull Donor—Acceptor Chromophores. J. Phys. Chem. C 2020, 124 (3), 2146–2159.
- (58) Hestand, N. J.; Spano, F. C. Expanded Theory of H- and J-Molecular Aggregates: The Effects of Vibronic Coupling and Intermolecular Charge Transfer. *Chem. Rev.* **2018**, *118* (15), 7069–7163.
- (59) Bardi, B.; Dall'Agnese, C.; Moineau-Chane Ching, K. I.; Painelli, A.; Terenziani, F. Spectroscopic Investigation and Theoretical Modeling of Benzothiadiazole-Based Charge-Transfer Chromophores: From Solution to Nanoaggregates. *J. Phys. Chem. C* **2017**, *121* (32), 17466–17478.
- (60) Jenekhe, S. A.; Osaheni, J. A. Excimers and Exciplexes of Conjugated Polymers. *Science* **1994**, *265* (5173), 765.
- (61) Flanders, N. C.; Kirschner, M. S.; Kim, P.; Fauvell, T. J.; Evans, A. M.; Helweh, W.; Spencer, A. P.; Schaller, R. D.; Dichtel, W. R.; Chen, L. X. Large Exciton Diffusion Coefficients in Two-Dimensional Covalent Organic Frameworks with Different Domain Sizes Revealed by Ultrafast Exciton Dynamics. J. Am. Chem. Soc. 2020, 142 (35), 14957–14965.